Fully Blind Electromagnetic Characterization of Deep Sub-Wavelength (λ/100) Dielectric Slabs With Low Bandwidth Differential Transient Radar Technique at 10 GHz

Ali Pourkazemi, Salar Tayebi, and Johan H. Stiens

***Abstract*— Transient radar method (TRM) is introduced as a novel non-destructive testing (NDT) technique that is capable of analyzing fully blindly and simultaneously the electromagnetic (EM) properties as well as geometric parameters of deep sub-wavelength thin single layer slabs. This study focuses on the minimum detectable layer thickness by means of TRM, which mainly depends on the experimental setup configuration. In this article, the complex permittivity and thickness of three polyvinyl chloride (PVC) sheets are extracted by means of a differential TRM set-up. The thickness of these PVC sheets was 1 mm, 500 μm, and 300 μm that corresponded to λ/30, λ/60, and λ/100, respectively (λ is the wavelength in free space). The carrier frequency was 10 GHz and the experiments were done in a bistatic radar setup. A differential TRM structure was used in this experiment. Some error sources, such as switch leakage and non-perpendicular illumination as well as systematic errors are considered as well. The experimentally obtained results are as follows: the thickness of these samples were 1033 ± 12, 535 ± 11, and 302 ± 9 μm with 1.18%, 0.94%, and 2.89% relative error, respectively. Additionally, the complex permittivity of these samples was found as (2.73 ± 0.02)–(0.23 ± 0.01)j, (2.70 ± 0.02)–(0.20 ± 0.02)j, and (2.65 ± 0.02)–(0.37 ± 0.01)j, respectively. This novel technique has the potential for deployment in a wide range of applications ranging from the piping, wind energy industry, and automotive to biotechnology, food industry, clinical monitoring, and pharmacy.**

***Index Terms*— Blind characterization, complex permittivity extraction, contact-free thickness measurement, microwave and millimeter wave (MMW), non-destructive testing (NDT), time-domain reflectometry (TDR), transient radar method (TRM), ultra-sub-wavelength depth resolution.**

Manuscript received March 20, 2021; revised June 18, 2021 and September 20, 2021; accepted November 29, 2021. Date of publication December 28, 2021; date of current version March 4, 2022. This work was supported in part by the Vrije Universiteit Brussel (VUB) through the SRP-Project M3D2 and the ETRO-IOF Project under Grant IOF3016 and Grant IOF242; in part by the OZR-FWO Hercules MZW equipment: GHz-THz measurement infrastructure, Innoviris-Brussels through the D-Stream Project under Grant BRGRD32; and in part by the Differential Smooth Transient Radar Method. *(Corresponding author: Ali Pourkazemi.)*

Ali Pourkazemi and Salar Tayebi are with the Department of Electronics and Informatics ETRO-IR, Faculty of Engineering, Vrije Universiteit Brussel, 1050 Brussels, Belgium (e-mail: apourkaz@etrovub.be; stayebi@etrovub.be).

Johan H. Stiens is with the Department of Electronics and Informatics ETRO-IR, Faculty of Engineering, Vrije Universiteit Brussel, 1050 Brussels, Belgium, and also with SSET, IMEC, 3001 Leuven, Belgium (e-mail: johan.stiens@vub.be).

Color versions of one or more figures in this article are available at https://doi.org/10.1109/TMTT.2021.3135356.

Digital Object Identifier 10.1109/TMTT.2021.3135356

I. Introduction

NON-DESTRUCTIVE testing (NDT) in the largest categorization can be divided into three parts which are techniques, materials, and conditions. Among various techniques, there is one group which is named wave-based techniques. For instance, X-ray imaging, ultrasonic investigation, laser pulse scanning, electromagnetic (EM) radiation, etc. are the main NDT methods that are categorized as wave-based techniques [1], [2]. In this group, using EM wave testing, in general, is implemented for monitoring physical and chemical changes of different industrial and pharmaceutical materials. Choosing the best frequency range in EM wave-based testing highly depends on the ultimate application, needed lateral resolution, and penetration depth. Consequently, microwave, millimeter wave (MMW), and THz technology have been used in different techniques and methodologies, such as spectroscopy, time-of-flight with respect to the pulse, time-domain reflectometry (TDR), frequency modulation continuous wave (FMCW), etc. Reviewing the recent scientific literature reveals that some typical MMW/THz devices and systems, as well as some engineering applications in composite material characterization, thermal barrier coatings, car paint films, marine protective coatings, noninvasive clinical monitoring, and pharmaceutical tablet coatings are growing rapidly [3]–[9]. Moreover, reviewing wave-based techniques shows sub-THz or THz imaging methods have higher resolution in comparison with ultrasound imaging technique, however, the penetration depth is lower [10]. Additionally, the necessity of couplant, priori knowledge, and generating ionizing radiation are the main disadvantages of ultrasonic wave, MMW/THz, and X-ray in traditional ways, respectively, [11]–[14]. A few years ago, Pourkazemi and Stiens [15] have patented a new EM radar-type wave-based technique, that is able to keep the advantages of traditional EM wave methods while it is completely blind. In other words, this method is fully independent of priori knowledge. This method was coined transient radar method (TRM). Radar techniques are one of the oldest techniques in NDT, but the TRM can be considered as a novel category aiming at NDT applications and operating in the time domain (i.e., a time of flight method). The significant difference between TRM and other time-based methods is the usage of narrowband illumination. Moreover,

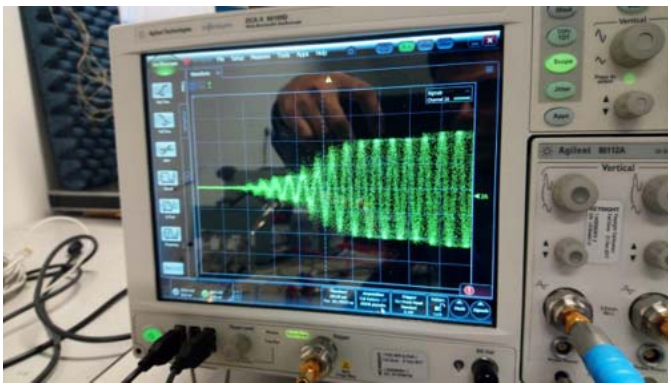

Fig. 1. Experimental transient radar signal. The carrier frequency, rise time, and bandwidth were 10 GHz, 1 ns, and less than 1 GHz, respectively.

due to dispersion characteristics (frequency-dependent EM properties) of materials, samples under test cannot be analyzed by traditional pulse-based systems without *a priori* knowledge. The latter is not always available. There is a solution to measure EM properties as well as the thickness of single-layer structures with a metallic surface in the back [17], however, for two or multilayer structures, it does not work. Ultimately, measuring the EM properties of thin layers in advance does not yield correct results due to the aforementioned interfacial issues. Hence, there is a huge need to develop a measurement tool to extract EM properties without *a priori* knowledge. Based on the research results that have been obtained in recent years, TRM is a promising method to achieve this goal in the near future. TRM can be categorized under TDR methods but without the need for an ultrashort broadband pulse.

In fact, transient radar signal is a time-dependent transient sinusoidal wave from no-radiation to steady-state condition, that stimulates narrow bandwidth (see Fig. 1). A transient sinusoidal wave is radiated toward the sample under test (SUT), subsequently, a time-dependent reflection trace will be recorded by single-shot samplers [15], [18], [19]. It is obvious that the receiver receives the nose of the reflection signal [head of the first propagation path (PP)] after the round-trip time (RTT) defined as the time to travel twice the distance between the emitter antenna and the SUT. The receiver keeps receiving signals as long as the signal generator is operating (see Fig. 2). This time-dependent reflection is generated by means of the accumulation of several time-dependent reflections which are created based on each PP.

Each PP is the one possibility that a wave can travel through it; the departure point is the transmitter antenna and the destination is the receiver. These PPs can be described by a unique set of equations with respect to the number of layers and EM properties of each layer. As the simplest case scenario, imagine there is a single-layer structure as the SUT, hence, the first PP is from the transmitter antenna toward the front side of the SUT and then reflection to the receiver. The second PP is from the transmitter antenna toward the SUT and passes from the front side toward the backside and the reflection from the backside and then passes again from the front side toward the receiver antenna. In transient time, all PPs from the various layer interfaces of the multilayer

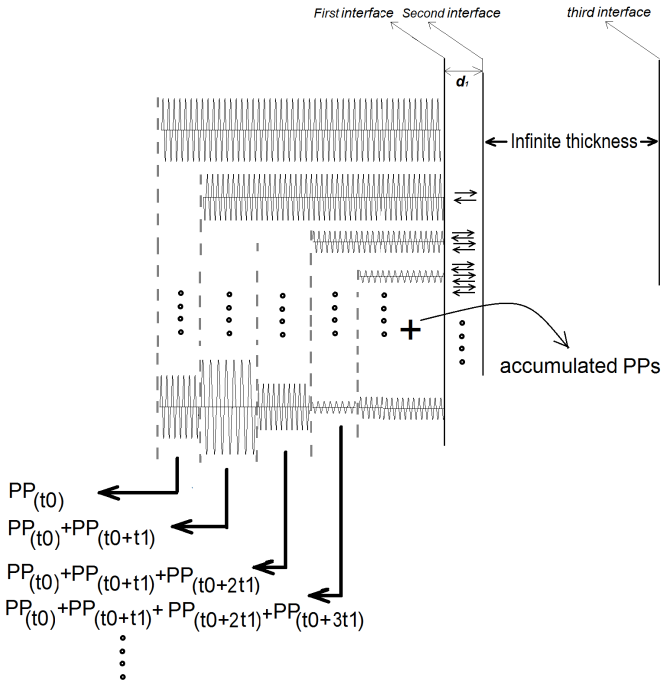

Fig. 2. Schematic illustration of the time evolution of the EM waves being reflected on the various interfaces of the multilayer structure. The nose of the illustrated reflected wave hits the detector after the first RTT.

structure are detectable except the ones with an amplitude within the noise level. In this article, at first, we consider that samples are homogeneous single-layer structures that are exposed in the air. We are going to measure the complex permittivity as well as thickness while the temperature is monitored. The main goal of this experiment was to investigate the possibility of detecting the EM characteristics as well as thickness of samples with a thickness of $\lambda/100$ or beyond. Because of the very thin layers, PPs are generated with very short time-delay with respect to each other. Hence, a small drift (few hundreds of picoseconds either from the oscilloscope or the single shot sampler) can create a significant error for calculating EM properties as well as thickness. To cope with drift, a differential system has been implemented instead of single-ended structure.

In the TRM method, the calibration is based on the recording of REF and AIR signals, where we refer to the reflected signal from a perfect smooth metallic reflector (PSMR) and the crosstalk of transmitter and receiver antennas without the presence of any object, respectively. During these measurements, these three signals drift with respect to each other. Ultimately differential system allows to overcome errors due to systematic error sources (see Fig. 3).

In the following sections, we describe the investigated samples, measurement procedure, error mitigation process, and the obtained results, respectively. Subsequently, a brief discussion regarding the obtained results, summary, and conclusion are provided as well in order to have an overview of this study.

II. Material and Methodology

Three semi-flexible polyvinyl chloride (PVC) sheets (50×30 cm) with a thickness of 1000, 500, and 300 μm,

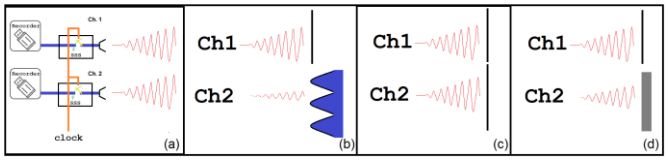

Fig. 3. Schematic illustration of the calibration procedure for the differential TRM set-up. (a) Two used receiver channels of the differential TRM set-up. (b) First step of the calibration procedure: AIR (channel 2) and PSMR (channel 1) measurements. (c) Second step of the calibration procedure: REF (PSMR in channel 2) and PSMR (channel 1) measurements. (d) Effective measurement step; SAM [reflected signal from sample under investigation, (channel 2)] and PSMR (channel 1) measurement.

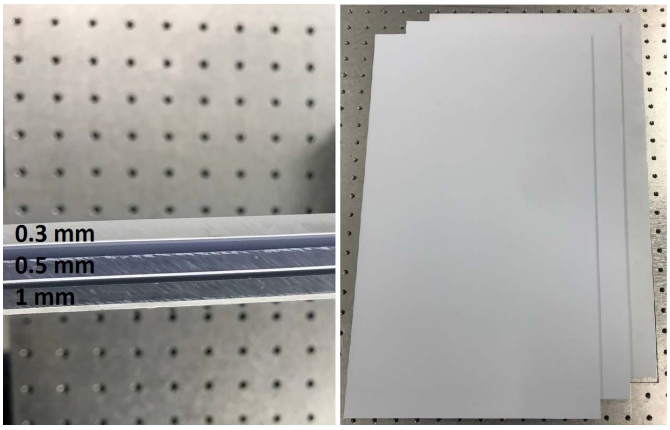

Fig. 4. PVC sheets that were used for this experiment.

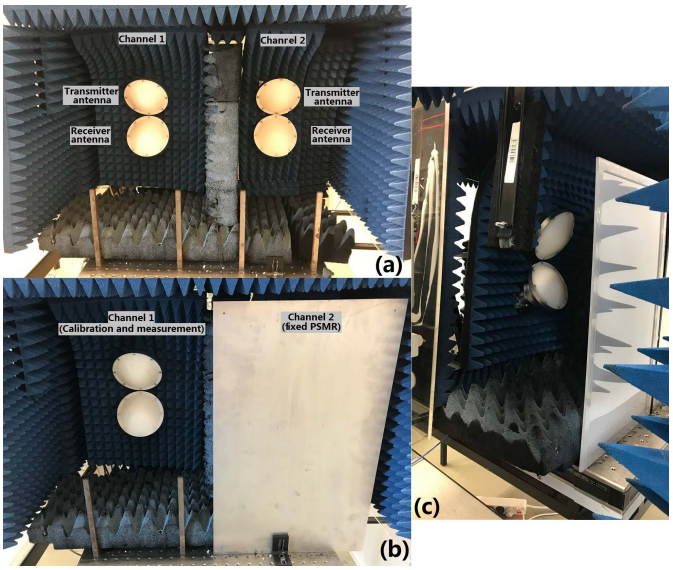

Fig. 5. Experimental 10 GHz differential TRM setup. (a) Differential structure comprising quasi-identical transmitter antenna and a receiver. (b) As shown, channel 1 is for the calibration and sample measurement, while channel 2 was used for drift detection and mitigation. (c) Rigid frames and sample holder to place the samples in smooth and perpendicular position with respect to the transmitter antenna.

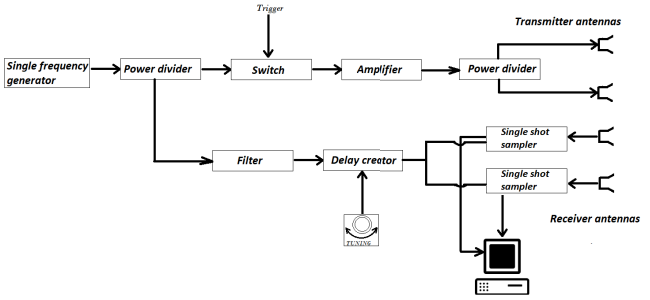

Fig. 6. Block diagram representing the TRM measurement set-up.

respectively, were selected. As the SUTs are illuminated in a vertical position, three rigid frames supported them (see Fig. 4). To mitigate the environmental interference, strong absorber sheets were placed behind the SUT (see Fig. 5). Since the main target of this experiment was the investigation of depth resolution with respect to the ability of TRM to measure thickness as well as EM properties of the SUT, the room temperature and humidity were kept constant during the measurements.

The differential structure was made by means of two separate channels. Each channel consists of a transmitter antenna and a receiver (see Fig. 5).

As illustrated in Fig. 6, the first module in the TRM measurement set-up is the single frequency generator. This is a narrowband voltage-controlled oscillator (VCO) that generates continuous EM waves. The power divider is the second module that functions as a power splitter that provides a similar (power) amplitude and phase to each port. The next module is the single pole single throw (SPST) switch. This switch has two functions in this set-up. The first task of the switch is to create on-off square signals comprising transient modes at the initial and terminal part; the second task, however, is to reflect a part of the illumination signal to trigger the single-shot sampler at the toggling moment from the conductive to the non-conductive state. It is obvious that the amplifier improves the signal-to-noise ratio (SNR) by increasing the magnitude of the radiated signal. The single-shot sampler or sample and hold module is the module that records the amplitude of the reflected EM waves during an infinitesimal time interval. Delay creator helps the operator to record the reflected signal at certain time-frames. Last, the trigger module sends the command to the SPST switch for toggling from non-conductive to conductive condition and vice versa. Actually, a sampling oscilloscope is the most suitable signal acquisition device for TRM not only for its repeatability but also because of the time resolution. Modern sampling oscilloscopes have a time resolution of few tens of femtoseconds which is necessary for TRM measurements since time resolution has a direct relation with depth resolution. Additionally, higher SNR of sampling oscilloscopes results in significantly more accurate results. Generally, the acquisition speed of TRM signal in the sampling oscilloscope is significantly smaller compared with the real time oscilloscopes. For instance, in a typical modern sampling oscilloscope, the sampling rate is around 50 KSa/s, but for a real time sampler, is 250 GSa/s, approximately. In the actual experiment, by means of a tuner, the time delay for both samplers was adjusted in a way to initiate the acquisition before the reflection of transient radar signals. In the next step, time resolution was adjusted to its minimum possible value.

In this measurement set-up, channel 1 was allocated to the recording of the time-dependent reflection signals from a fixed PSMR in order to mitigate drift. Channel 2 was deployed for

calibration steps as well as the sample measurements (see Fig. 3). Consequently, four reflected signals were recorded for the two-step calibration process; channel 1 received two reflections from PSMR while channel 2 received one reflection from the PSMR and one from air (AIR trace). Finally, with respect to investigations on the SUT, channel 1 was used to record the PSMR reflection while channel 2 was used for the sample investigation.

In general, in TRM, the peeling method can be used to analyze the reflection signal traces, however, since we assumed that the samples are homogenous, we processed the signals as follows.

1) At the first stage, histogram technique was used to convert the raw signals into the smooth ones. In fact, areas with the highest density of sample points in amplitude-time plane were determined by means of density-weighted averaging technique. The averaging process was restricted to ten measurements to avoid drift phenomena in the circuit [15].
2) Drift in channel 1 was calculated for each step of the experiment. Each step was named according to the sample in front of channel 2. For instance, AIR indicates measuring the reflection signal from the fixed PSMR in channel 1, while nothing is placed in channel 2. Similarly, REF indicates measuring the reflection signal from PSMR in front of channel 1, while another PSMR is placed in front of channel 2. Last, SAM (reflected signal from sample under investigation) indicates measuring the reflection signal from PSMR in channel 1, when the PVC sheets are placed in channel 2.
3) The calculated drift (calculated and evaluated all the time) from channel 1 was applied to the recorded signals from channel 2. Consequently, from this moment onward, we only work with three recorded signals from channel 2.
4) In order to remove the crosstalk between antennas and to have pure reflection signals, AIR signal was subtracted from REF and SAM signals.
5) Last, we reconciled the REF and AIR signals in order to find the nose of the signal. Nose of the signal indicates the transient reflection signal from the shortest RTT between the transmitter antenna and the front side of the SUT.
6) To extract the complex permittivity, at first, we should decompose SAM-AIR couple trace into the PPs. Subsequently, the first PP which is named $\mathrm{PP}_{(t0)}$ can be obtained by trial and error to find amplitude and phase change in the REF-AIR signal and reconcile it as much as possible to the SAM-AIR signal

$$\mathrm{PP}_{(t0)} = A\Gamma_{01}e^{-j2\beta_0 d_0}e^{j\omega_0 t}U(t-t_0), \quad t > t_0 \tag{1}$$

where A, Γ_{01}, β_0, d_0, ω_0, t, t_0, $U(t)$, and $\mathrm{PP}_{(t0)}$ refer to the amplitude, reflection coefficient from the front side, propagation constant in free space, the distance between antennas and SUT, angular frequency, time, RTT between the antennas and SUT, Heaviside function, and first PP, respectively. In other words, $\mathrm{PP}_{(t0)}$ is exactly, such as the REF-AIR signal multiplied by an unknown complex coefficient. Consequently, finding this unknown complex coefficient results in finding the reflection coefficient of the first layer (Γ_{01}). Eventually, the complex permittivity will be obtained according to Γ_{01} and magnetic permeability (μ_0).

7) By subtracting $\mathrm{PP}_{(t0)}$ from SAM-AIR signal, we can extract the second PP ($\mathrm{PP}_{(t0+t1)}$) for a double or multilayer structure. Extraction of this PP leads to the reflection coefficient of the second layer (Γ_{12}). However, for a single-layer structure, Γ_{12} is known. Since $\mathrm{PP}_{(t0)}$ and $\mathrm{PP}_{(t0+t1)}$ are the PPs from the first and second surfaces of the SUT, we can calculate the thickness based on the difference between these two PPs

$$\mathrm{PP}_{(t_0+t_1)} = \left(\frac{\mathrm{PP}_{(t_0)}}{\Gamma_{01}}\right)T_{01}T_{10}e^{-2\alpha_1 d_1}e^{-2j(\beta_0 d_0+\beta_1 d_1)} .\Gamma_{10}e^{j\omega_0 t}U(t-t_0-t_1), \quad t > t_0+t_1 \tag{2}$$

where T_{01}, T_{10}, β_1, d_1, t_1, and α_1 refer to the transmission coefficient through the first interface, transmission coefficient through the second interface, propagation constant in the material, thickness of SUT, RTT in sample, and attenuation coefficient in sample, respectively.
We can follow this algorithm to calculate other PPs ($\mathrm{PP}_{(t0+nt1)}$) for a multilayer structure (see Fig. 7)

$$\mathrm{PP}_{(t_0+nt_1)} = \left(\frac{1}{\mathrm{PP}_{(t_0)}}\right)^{n-1} \times \left(\frac{1}{T_{01}T_{10}}\right)^{n-1} \times (\mathrm{PP}_{(t_0+t_1)})^n .U(t-t_0-nt_1), t > t_0+nt_1. \tag{3}$$

This is obvious that some of them can be calculated according to the previous ones while some of them should be obtained by means of trial and error in the mentioned algorithm for multilayer structures.

8) For very thin structures, the time delay between PPs is relatively small. Therefore, extraction of PPs would be

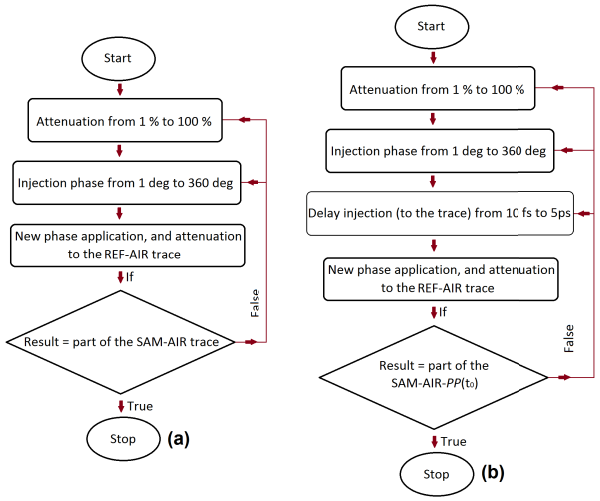

Fig. 7. Flowchart explaining the extraction of PPs. (a) First PP which is named $\mathrm{PP}_{(t0)}$ can be obtained by trial and error to find amplitude and phase change in the REF-AIR signal and reconcile it as much as possible to the SAM-AIR signal. In other words, $\mathrm{PP}_{(t0)}$ is exactly, such as REF-AIR signal multiplied by an unknown complex coefficient. (b) By subtracting $\mathrm{PP}_{(t0)}$ from SAM-AIR signal and applying the same principle as (a), we can extract $\mathrm{PP}_{(t0+t1)}$ as a PP for a double or multilayer structure.

challenging. Consequently, we extract four or five PPs and implement a cost function based on the following algorithm:

$$\sum_{n=0}^{n=4} \mathrm{PP}_{(t0+nt_1)} - (\mathrm{SAM} - \mathrm{AIR}). \tag{4}$$

Since the nose of the signal is already obtained, there are only three unknown parameters to be calculated: the complex permittivity and thickness of the single-layer structure.

Although there is a big gap between the actual model and the above formulas, they still show the physical process that takes place between transient incidence as well as the single-layer structure. For instance, in these formulas, it is assumed that the rise time is generated as a pure and zero harmonic, however, this is not the case in reality. In general, the PPs are completely dependent on each other. In other words, if we obtain the first one correctly, others will be derived correctly as well. Due to complex transient dynamics of the switch toggling from off-to-on, the whole mathematical operations, such as phase shift, attenuation coefficient, as well as time delay should be applied to each point of the traces.

III. Error Mitigation

To calculate the complex permittivity as well as thickness with high accuracy, error mitigation is needed to be considered. There are several kinds of error sources that can affect more or less the accuracy of the final results. The amount of impact of each error source depends on the electronic specifications as well as geometric and EM properties of the SUT. For instance, when the thickness of the sample under investigation is relatively lower than the wavelength, the divergence error [20] can be neglected. However, for such kind of SUT which is of homogeneous thin single-layer structures, only one considers the following important error sources.

Switch-leakage error: since the switch used in this study does not create infinite insulation there is even radiation leaking to the SUT when the switch is in its non-conductive mode. Therefore, switch leakage error should be taken into account. Furthermore, the angle between the transmitter and receiver antenna can potentially lead to an increasing RTT in the body of sample. Additionally, the EM properties must be calculated based on the polarization of the incident wave in Fresnel equations [20]. Finally, the finite conductivity of PSMR at 24 °C should be considered as well [20]. Ultimately, drift as a stochastic error source should be resolved too.

As illustrated in Fig. 8, at first, we assume that the real thickness and complex permittivity of the SUT are 1 mm and 2.73–0.02j, respectively. Afterward, by considering different values for thickness and complex permittivity, the PPs have been re-calculated to investigate the amount of error due to the thickness and complex permittivity changes as a function of PPs. As shown in Fig. 8, transient radar signal is more sensitive to thickness compared with sensitivity to the absolute value of permittivity. In other words, uncertainty in thickness calculation is smaller than uncertainty in the absolute value of permittivity.

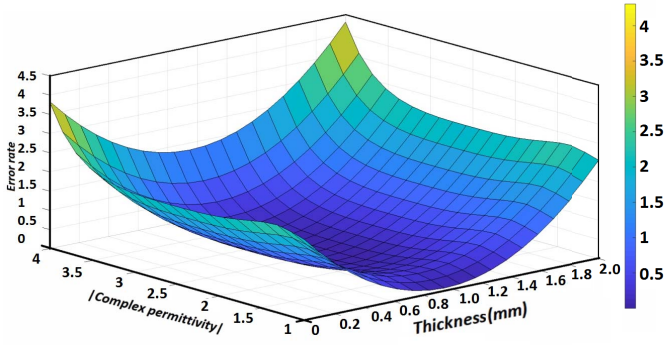

Fig. 8. Sensitivity of transient radar signal with respect to thickness and absolute value of complex permittivity.

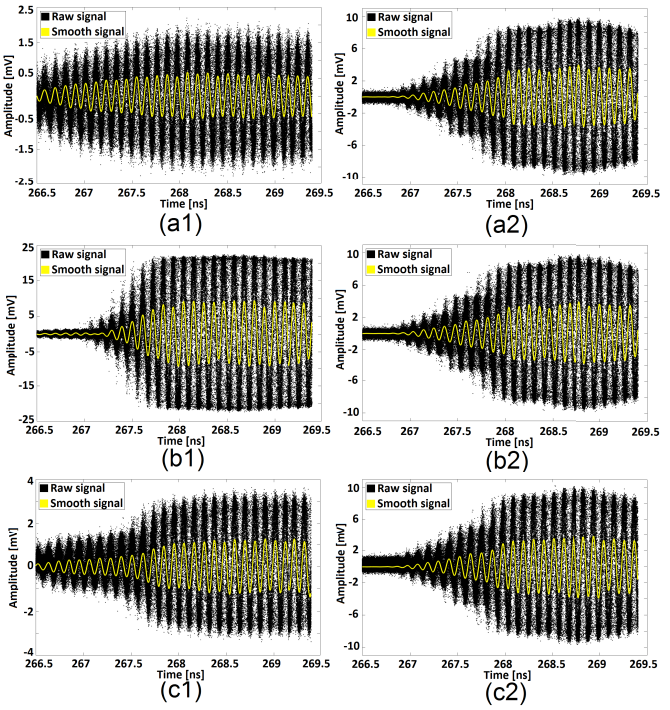

Fig. 9. Recorded signals from the two-step calibration procedure and one-step measurement. (a1) and (a2) Recorded traces of AIR and PSMR from channel 2 and 1, respectively. (b1) and (b2) Recorded traces of REF (PSMR) and PSMR from both channels. (c1) and (c2) Recorded traces of SAM and PSMR from channel 2 and 1.

IV. Result and Discussion

In this experiment, each PVC sheet was investigated three times. Subsequently, by means of the histogram technique, smooth traces of air (AIR), PSMR (REF), and the SUT (SAM) were generated for further signal processing. In the next step, we calculated the drift based on the results achieved from channel 1 and applied it to channel 2. Therefore, the nose region was determined by means of reconciling the AIR and REF traces from channel 2. Afterward, the peeling method with an appropriate algorithm was performed in order to find PPs. Finally, the thickness and dielectric permittivity were extracted according to the PPs.

In Fig. 9, results of the two-step calibration procedure, as well as the measurements, are presented. As illustrated, at each stage, we recorded the reflection from channels 2 and 1 in order to cope with the drift issue.

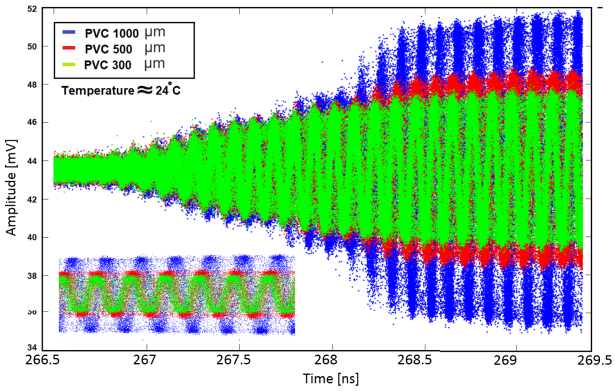

Fig. 10. Time dependent reflection signals from three different thicknesses of PVC sheets at a laboratory temperature of 24 °C (SAM signal).

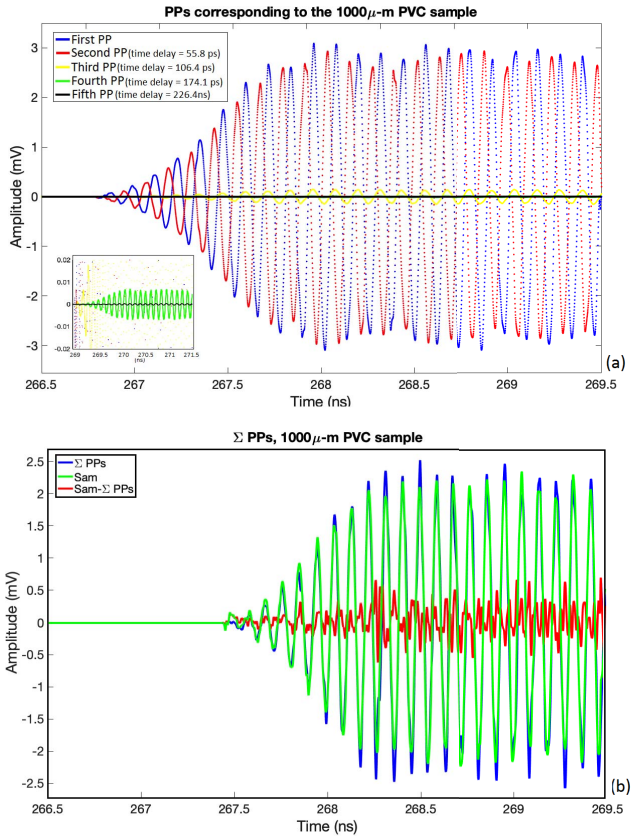

Fig. 11. Illustration of PPs. (a) Five PPs for the PVC sheet with the thickness of 1021 μm. (b) Subtraction of the collected PPs from SAM-AIR trace according to the cost function.

In Fig. 10, there is a visual comparison between three traces that are generated by TRM signals from three PVC sheets with different thicknesses. As can be seen, the nose of the signal represents the first PP received from the front side of the sample under investigation.

After a certain time (for instance, 268.3 ns for the sample with the thickness of 1 mm) a sharp increase in the signal can be seen which refers to the second PP received from the backside of the SUT. Five consecutive PPs which are related to the SUT with 1 mm thickness are shown in Fig. 11(a). Additionally, the SAM signal of the sample with 1 mm thickness, the summation of its PPs [Fig. 11(a)], and the subtraction of these PPs from SAM-AIR signal is shown in Fig. 11(b). The important thing to be pointed out is that the first and second PPs are significantly larger than the noise level and are clearly distinguishable in Fig. 11(a). However, the rest of the PPs is below the noise level and cannot be analyzed further.

TABLE I

EXPERIMENTAL RESULTS OF THREE PVC SHEETS WITH DIFFERENT THICKNESSES, DETERMINED VIA CALIPER AS WELL AS TRM AT A LABORATORY TEMPERATURE OF 24 °C

PVC-sample thickness range (μm)	Temperature (°Celcius)	Thickness Via caliper (μm)	Thickness Via TRM (μm)	Complex permittivity	Relative error for thickness (%)
+/- 1000	24	1021±139	1033±12	(2.73±0.02)-(0.23±0.01)j	1.18
+/- 500	24	530±78	535±11	(2.70±0.02)-(0.20±0.02)j	0.94
+/- 300	24	311±39	302±09	(2.65±0.02)-(0.37±0.01)j	2.89

The final results achieved from this experiment are presented in Table I.

As can be seen in Table I, the temperature during the investigation was kept constant as much as possible to prevent any additional error source. The thickness of the PVC sheets was measured five times by means of a caliper. Subsequently, the mean and standard deviation of each PVC layer thickness were calculated. The thickness of the PVC sheets measured by a caliper was 1021 $\pm$ 139, 530 $\pm$ 78, and 311 $\pm$ 39 μm. On the other side, the thickness measured by TRM was 1033 $\pm$ 12, 535 $\pm$ 11, and 302 $\pm$ 9 μm, respectively. Comparing the premeasured thickness values with the obtained ones, resulted in finding the relative error for each sample, which was 1.18%, 0.94%, and 2.89%, respectively. With respect to the complex permittivity, the results were (2.73 $\pm$ 0.02)–(0.23 $\pm$ 0.01)j, (2.70 $\pm$ 0.02)–(0.20 $\pm$ 0.02)j, and (2.65 $\pm$ 0.02)–(0.37 $\pm$ 0.01)j for the samples with a thickness of approximately 1000, 500, and 300 μm, respectively.

V. SUMMARY AND CONCLUSION

For the first time ever, we were able to design, assemble, and test a differential TRM system, operating at 10 GHz allowing to evaluate the full potential of TRM to characterize subwavelength structures in a totally blind way. The advanced proprietary algorithms have been implemented to mitigate drift error that leads to larger errors, specifically for single thin layer structures. This technique allowed us to characterize fully blindly a dielectric layer structure with a thickness of λ/100 with a relative error smaller than 3%. As explained in this study, thicknesses of the PVC sheets measured by a caliper were 1021 $\pm$ 139, 530 $\pm$ 78, and 311 $\pm$ 39 μm, on the other hand, the measured thicknesses via TRM were 1033 $\pm$ 12, 535 $\pm$ 11, and 302 $\pm$ 9 μm with 1.18%, 0.94%, and 2.89% relative error, respectively. In general, the minimum detectable layer thickness depends on several factors including the vertical resolution of oscilloscope, SNR, noise level, carrier frequency, EM properties of SUT, etc. The obtained complex permittivity values by means of TRM were (2.73 $\pm$ 0.02)–(0.23 $\pm$ 0.01)j, (2.70 $\pm$ 0.02)–(0.20 $\pm$ 0.02)j, and (2.65 $\pm$ 0.02)–(0.37 $\pm$ 0.01)j for the PVC sheets, independently. The complex permittivity is highly dependent on the composition of the sample under investigation. Therefore, different values

of permittivity can be found in different studies depending on the molecular composition of PVC samples. For instance, the dielectric properties of various polymers including PVC have been investigated by means of dynamic-electric analysis (DEA) in 2013 [21]. Since the samples investigated in this study have been reinforced with ground tire rubber (GTR), the obtained permittivity values are not exactly the same as the results of this study, however, the obtained permittivity values by means of TRM are relatively in agreement with the previously reported ones. In the future, TRM will be implemented at higher frequencies up to 100 GHz, in a differential set-up that leads to higher precision and depth resolution in addition to lateral resolution. Moreover, the new algorithm which is able to extract complex permittivity and geometric information for thin multilayer structures by means of transient radar signal will be presented as well.

REFERENCES

[1] S. Gholizadeh, "A review of non-destructive testing methods of composite materials," *Proc. Struct. Integrity*, vol. 1, pp. 50–57, Jan. 2016.

[2] G. V. Subbarao and R. Mulaveesala, "Quadratic frequency modulated thermal wave imaging for non-destructive testing," *Prog. Electromagn. Res. M*, vol. 26, pp. 11–22, 2012.

[3] M. Tani *et al.*, "Efficient electro-optic sampling detection of terahertz radiation via Cherenkov phase matching," *Opt. Exp.*, vol. 19, no. 21, pp. 19901–19906, 2011.

[4] Y. U. Jeong *et al.*, "First lasing of the KAERI compact far-infrared free-electron laser driven by a magnetron-based microtron," *Nucl. Instrum. Methods Phys. Res. A, Accel. Spectrom. Detect. Assoc. Equip.*, vol. 475, nos. 1–3, pp. 47–50, 2001.

[5] E. R. Brown, K. A. McIntosh, K. B. Nichols, and C. L. Dennis, "Photomixing up to 3.8 THz in low-temperature-grown GaAs," *Appl. Phys. Lett.*, vol. 66, no. 3, pp. 285–287, 1995.

[6] M. Tonouchi, "Cutting-edge terahertz technology," *Nature Photon.*, vol. 1, no. 2, pp. 97–105, 2007.

[7] P. Gu, M. Tani, M. Hyodo, K. Sakai, and T. Hidaka, "Generation of cw-terahertz radiation using a two-longitudinal-mode laser diode," *Jpn. J. Appl. Phys.*, vol. 37, pp. L976–L978, Aug. 1998.

[8] J. H. Smet, C. G. Fonstad, and Q. Hu, "Intrawell and interwell intersubband transitions in multiple quantum wells for far-infrared sources," *J. Appl. Phys.*, vol. 79, no. 12, pp. 9305–9320, Jun. 1996.

[9] Y. C. Shen, P. C. Upadhya, E. H. Linfield, H. E. Beere, and A. G. Davies, "Terahertz generation from coherent optical phonons in a biased GaAs photoconductive emitter," *Phys. Rev. B, Condens. Matter*, vol. 69, no. 23, pp. 235–325, Jun. 2004.

[10] S. C. Zhong, "Progress in terahertz nondestructive testing: A review," *Frontiers Mech. Eng.*, vol. 14, pp. 273–281, Sep. 2019.

[11] J. R. Little, "High-resolution, nondestructive imaging of dielectric materials," U.S. Patent 0 283 483, Nov. 11, 2010.

[12] J. R. Little, "Interferometric localization of irregularities," U.S. Patent 6 653 847, Nov. 25, 2003.

[13] K. L. Lewotsky, "Terahertz's penetrating appeal," *SPIE Newsroom*, vol. 1, no. 2, 2006.

[14] I. Amenabar, F. Lopez, and A. Mendikute, "In introductory review to THz non-destructive testing of composite mater," *J. Infr., Millim., THz Waves*, vol. 34, no. 2, pp. 152–169, Feb. 2013.

[15] A. Pourkazemi and J. Stiens, "Characterization of multilayer structures," European Patent 3 106 861 A1, Jun. 19, 2015.

[16] Y. Dong, S. Lawman, Y. Zheng, D. Williams, J. Zhang, and Y.-C. Shen, "Nondestructive analysis of automotive paints with spectral domain optical coherence tomography," *Appl. Opt.*, vol. 55, no. 13, p. 3695, 2016.

[17] F. Vandrevala and E. Einarsson, "Decoupling substrate thickness and refractive index measurement in THz time-domain spectroscopy," *Opt. Exp.*, vol. 26, no. 2, pp. 1697–1702, 2018.

[18] A. Pourkazemi, W. Ranson, J. Stiens, M. Becquaert, and M. Vandewal, "Novel illumination and parameter extraction technique for the characterization of multilayer structures in the GHz range with deep subwavelength resolution," in *Proc. IEEE 15th Medit. Microw. Symp. (MMS)*, Nov. 2015, pp. 1–4.

[19] A. Pourkazemi, J. H. Stiens, M. Becquaert, and M. Vandewal, "Transient radar method: Novel illumination and blind electromagnetic/geometrical parameter extraction technique for multilayer structures," *IEEE Trans. Microw. Theory Techn.*, vol. 65, no. 6, pp. 2171–2184, Jun. 2017.

[20] A. Pourkazemi, S. Tayebi, and J. H. Stiens, "Error assessment and mitigation methods in transient radar method," *Sensors*, vol. 1, no. 1, p. 263, 2020.

[21] R. Mujal-Rosas, M. Marin-Genesca, and J. Ballart-Prunell, "Dielectric properties of various polymers (PVC, EVA, HDPE, and PP) reinforced with ground tire rubber (GTR)," *Sci. Eng. Compos. Mater.*, vol. 22, no. 3, pp. 231–243, 2015.

Ali Pourkazemi received the M.Sc. degree in wave communication and bioengineering from KNT University, Tehran, Iran, in 2008, and the Ph.D. degree in wave communication and bioengineering from VUB, Brussels, Belgium, in 2017.

He has been working as a Post-Doctoral Researcher with the Department of Electronics and Informatics (ETRO-VUB) since 2017. He was selected as the Chief Technical Officer (CTO) of the project titled "Differential Smooth Transient Radar Method for Industry 4.0" by Innoviris (Financial institute to support patents in Brussels-Capital Region) in 2020. His major research interests are micro millimeter-wave and terahertz specifically, sensory applications indoor and in free-space, in time and frequency domain. Other interesting topics are related to Graphene, metamaterials, and biomaterials characterization. Time-domain reflectometry, ground-penetrating radar, RF circuits, and antennas for microwave millimeter wave THz are other fascinating topics. In electronic and signal processing field, interesting topics are measuring signal with picosecond, and femtosecond time resolution range. sample and hold circuits and modules in sub-THz range, time delay generator with optical path variation in picosecond and sub-picoseconds range, synchronization with indirect triggering exactly in 79 GHz, and random sample processing.

Salar Tayebi received the B.Sc. degree in biomedical engineering from the Amirkabir University of Technology (Tehran Polytechnic), Tehran, Iran, in 2016, and the M.Sc. degree in biomedical engineering from Vrije Universiteit Brussel, Brussels, Belgium, in 2021, where he is currently pursuing the Ph.D. degree.

He is currently a member of the Department of Electronics and Informatics (ETRO) of Vrije Universiteit Brussel. His main research topics are microwave reflectometry, transient radar method, noninvasive measurement techniques, and intra-abdominal pressure measurement. At the time being, he is working on noninvasive intra-abdominal pressure measurement by means of time-domain reflectometry.

Mr. Tayebi is a member of the European Society of Intensive Care Medicine (ESICM).

Johan H. Stiens received the electromechanical engineering degree in applied physics and the Ph.D. degree (Hons.) from the Faculty of Engineering Sciences, Universiteit Brussel (VUB), Brussels, Belgium, in 1990 and 1996, respectively.

Since 2011, he has been a Professor with the Department of Electronics and Informatics, VUB. He teaches several courses of the Engineering Science Faculty of three universities (VUB, ULB, and UGENT) ranging from micro-, nano-, and opto- and bio(medical) electronics, semiconductor devices, and related fabrication technologies, and modeling of physiological systems. He is the Vice-Chairman of the interuniversity Master program in biomedical engineering organized between UGENT and VUB. For about two decades, his research domain comprises the study of passive and active devices and systems operating in the 10 GHz to 30 THz range targeting sensing, imaging, and modulation functionalities. He has authored one book on GaN related semiconductor devices and of more than 300 (including +165 ISI) international journal and conference papers. He holds 13 patents with three pending. He has a strong focus on the valorization of research and development results when appropriate, resulting in the founding of two spinoff companies.